R/V Neil Armstrong Cruise Report
Voyage AR35-04

Reykjavik, Iceland to Reykjavik, Iceland
24-June-2019 to 29-July-2019

Formation and Elimination of Segmentation and Transform Faults on the Reykjanes Ridge

Fernando Martinez
Chief Scientist & Principal Investigator
Hawaii Institute of Geophysics and Planetology
School of Ocean and Earth Science and Technology
University of Hawaii at Manoa

Richard Hey
Co-Principal Investigator
Hawaii Institute of Geophysics and Planetology
School of Ocean and Earth Science and Technology
University of Hawaii at Manoa

Ármann Höskuldsson
Co-Chief Scientist
Faculty of Earth Sciences
University of Iceland

R/V NEIL ARMSTRONG AR35-04 PERSONNEL

Science Party

1. Fernando Martinez, Chief Scientist, Hawaii Institute of Geophysics and Planetology, School of Ocean and Earth Science and Technology, University of Hawaii at Manoa
2. Ármann Höskuldsson, Co-Chief Scientist, University of Iceland, Faculty of Earth Sciences
3. Sigvaldi Thordarson, ISOR, Iceland Geosurvey
4. Melissa Anderson, University of Toronto
5. Talia Moum, University of Toronto
6. Jacob Detrick Cooper, MATE Intern
7. Ella Cedarholm, MATE Intern
8. Lila Bellucci, MATE Intern
9. Daniel Thorhallsson, Hawaii Institute of Geophysics and Planetology and Department of Earth Sciences, School of Ocean and Earth Science and Technology, University of Hawaii at Manoa
10. Dominik Palgan, InterRidge Young Scholar, Poland,
11. Oriol Vilanova Pagès, University of Iceland
12. Teresa Martinez Perez, University of Iceland
13. Julia Urpi Badell, University of Iceland
14. Nicolas Levillayer, University of Iceland
15. Linus Hüne, University of Iceland
16. Maria Repczyńska, University of Iceland
17. Geoffrey Mibei, University of Iceland

Marine Technicians (Shipboard Science Support Group)

1. Cris Seaton
2. Becca Hudak

Officers and Crew

1. Kent Sheasley, Master
2. Mike Singleton, Chief Mate
3. Joshua Woodrow, Second Mate
4. Mariah Kopec-Belliveau, Third Mate
5. Scott Loweth, Boatswain
6. Kevin Roth, Able-Bodied Seaman
7. Lia Stamatiou, Able-Bodied Seaman
8. Paul Harris, Able-Bodied Seaman
9. Pete Marczak, Chief Engineer
10. Nickolas Alexander, First Assistant Engineer
11. Vasile Tudoran, Second Assistant Engineer
12. Isaac Cardosa, Third Assistant Engineer
13. Jay Pierce, Electrician
14. Kyle Covert, Oiler
15. Nick Clark, Oiler
16. Peter Gimiewicz, Oiler
17. Eric Whitte, Chief Steward
18. Brian Keenan, Cook
19. Thomas Leong, Mess Attendant
20. Brooke, Wagstaff, OS/Cadet

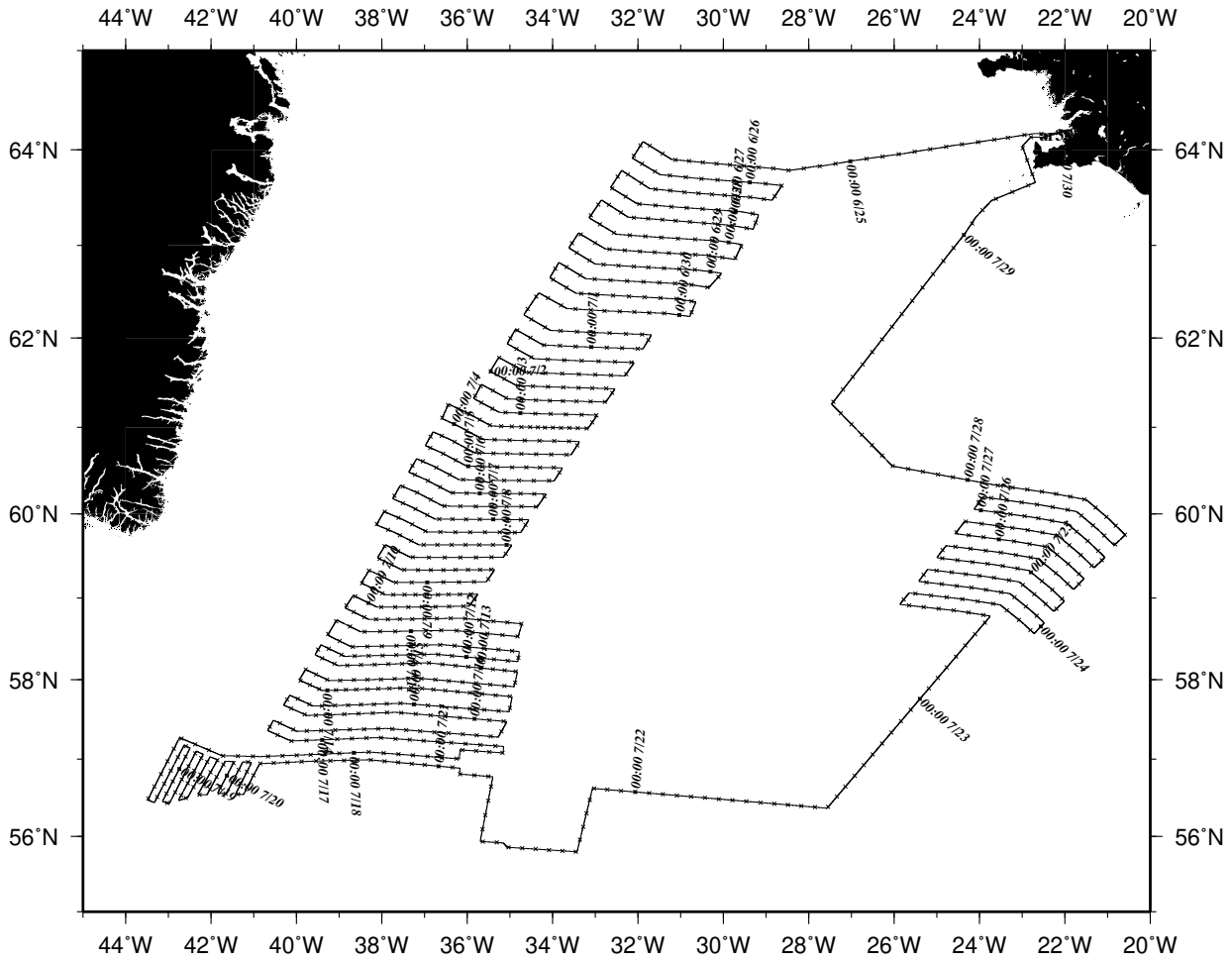

Figure 1. *R/V Neil Armstrong* ship track with annotated days and hour tick marks. Times are Universal Time Coordinated (UTC). Distance traveled was 8535 nautical miles (15,807 km) over 843 hours (35 days, 3 hours) at an average speed of 10.1 knots (5.2 m/s).

Overview and Scientific Objectives

The objectives of *R/V Neil Armstrong* cruise AR35-04 (Fig. 1) were to survey the flanks of the Reykjanes Ridge and determine the timing, geometry and associated geophysical characteristics of the large-scale tectonic reorganizations that occurred there in the Paleogene and continue to the present (Fig. 2). The North Atlantic plate boundary between what is today the Bight Fracture Zone and Iceland, a distance of nearly 1000 km, was originally a linear orthogonally-spreading ridge that became abruptly fragmented in a stair-step fashion following a change in plate motion [*Smallwood and White*, 2002]. Its subsequent evolution involved the systematic and progressive removal of offsets from north to south to re-establish its original linear configuration [*Hey et al.*, 2016; *Martinez and Hey*, 2017], even though this required the ridge to then spread obliquely, since the new spreading direction remained stable. These tectonic reorganizations took place within the region of influence of the Iceland "hotspot" which creates a strong gradient in mantle melting along the ridge, increasing crustal thicknesses by ~3-4 km

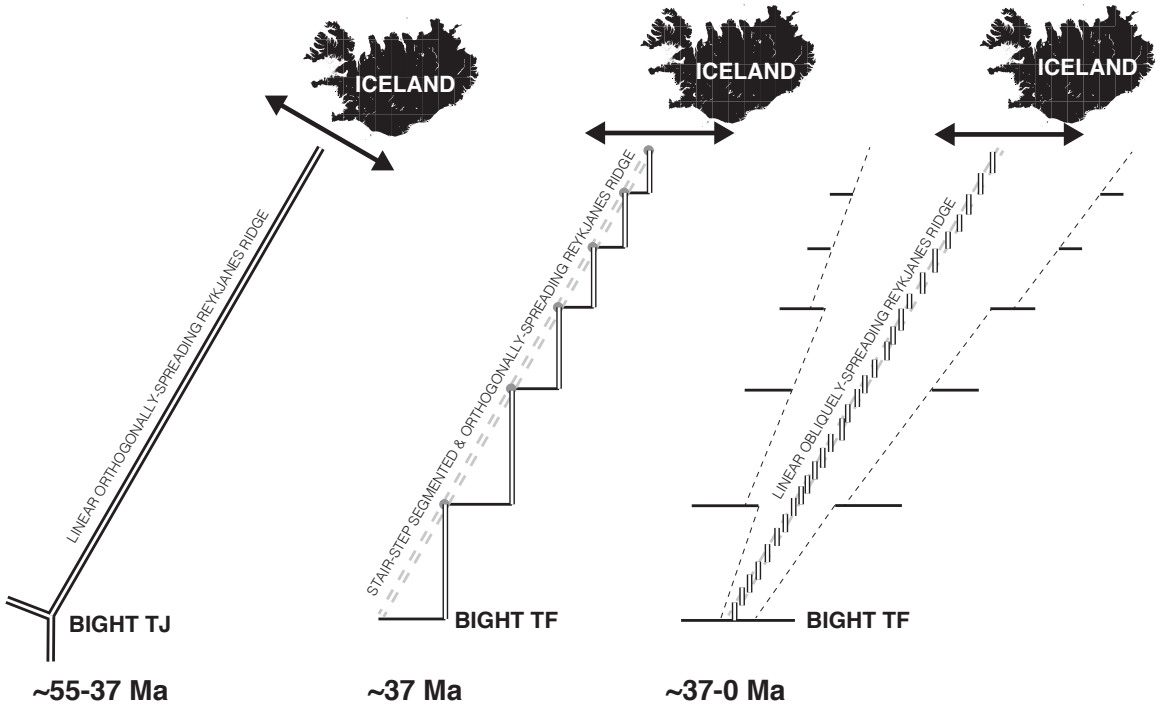

Figure 2.) Generalized depiction of the large-scale tectonic reconfigurations of the Reykjanes Ridge. Iceland is shown schematically for geographic reference only as it evolved as part of the Greenland-Iceland-Faroe Ridge during this time. Left panel: The Reykjanes Ridge originated as the approximately linear and orthogonally-spreading Greenland-Eurasia plate boundary following continental breakup (~55 Ma) and formed one arm of a ridge-ridge-ridge triple junction with the Labrador Sea spreading center to the west (the Greenland-North America plate boundary) and the Mid-Atlantic ridge to the south (the North America-Eurasia plate boundary). Middle panel: Around anomaly 17 (~37 Ma) the Labrador Sea spreading center failed joining Greenland to North America resulting in an abrupt ~30° change in opening direction across the Reykjanes Ridge. The Reykjanes Ridge broke up into a series of offset stair-step segments orthogonal to the new opening direction (former axis shown as gray dashed lines). The segments appear to have been longer with larger offsets to the south. Right panel: Promptly after forming, the ridge began to reconfigure back to its original linear geometry, eliminating the transform faults and offsets and re-establishing its original linear axis, even though this now required it to spread obliquely as the opening direction remained stable following the ~37 Ma change. Oblique spreading was accommodated by an *en echelon* array of right-stepping axial volcanic ridges within the new oblique plate boundary zone. As the ridge diachronously removed the offsets and became linear again from north to south, the prior fracture zones were left as fossil features on the ridge flanks.

and decreasing ridge axis depths by ~ 3000 m between the Bight Fracture Zone and Iceland [*Louden et al.*, 2004]. A mantle gradient in melting properties (compositional and/or thermal) is presumably what results in the regional residual basement depth anomaly that extends throughout this region of the North Atlantic from the Greenland-Iceland-Faroe Ridge to south of the Bight Fracture Zone. This gradient in mantle properties with distance from the Iceland hotspot apparently had strong modulating effects on the tectonic reorganizations: the initial

segment lengths and offsets appear in regional magnetic anomaly and satellite-derived gravity maps to be smaller toward Iceland and the segments evolved to re-establish the linear ridge configuration more quickly to the north [*Hey et al.*, 2016]. As both kinematic and "hotspot" effects influence their development, the Reykjanes ridge flanks are key areas for investigating lithospheric and mantle controls on ridge segmentation, formation and elimination of transform faults and the mechanisms controlling their evolution.

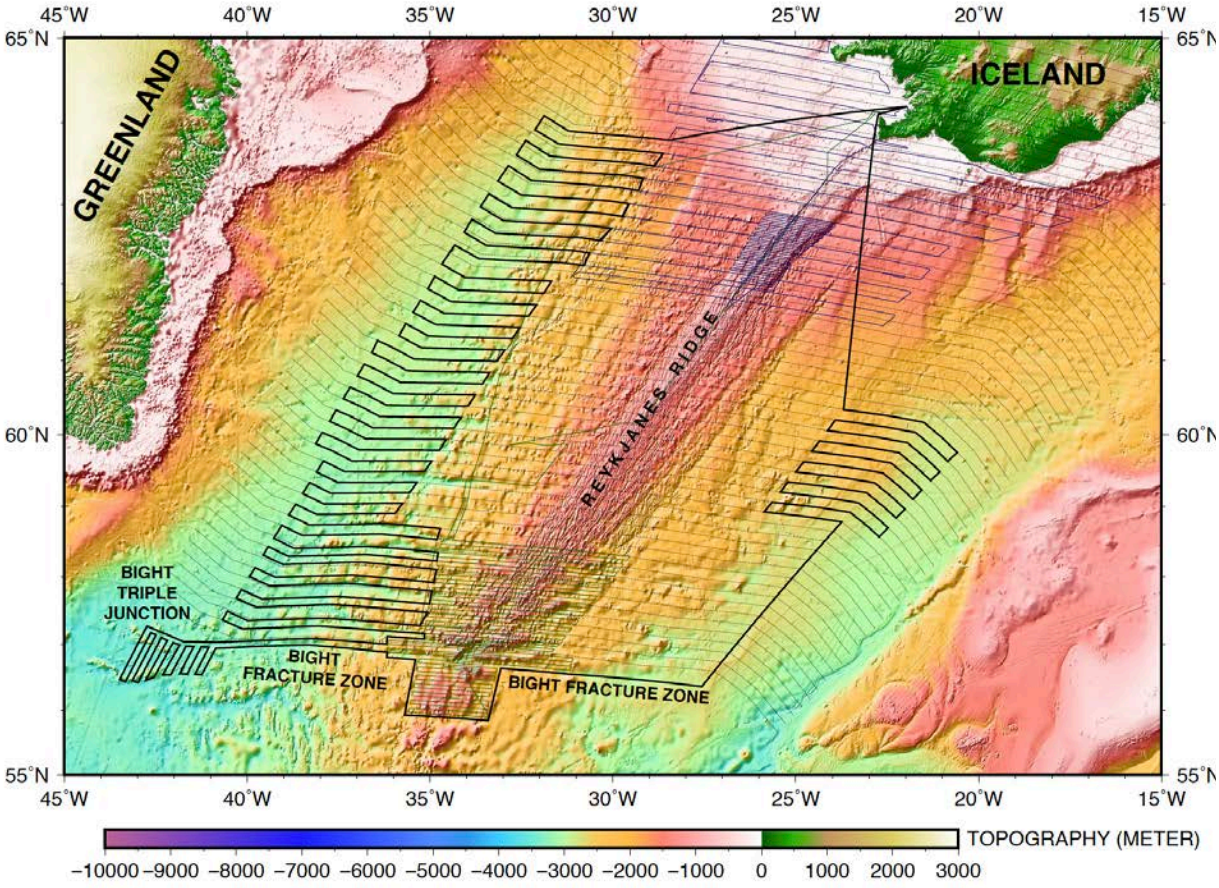

Figure 3) Survey track overlaid on SRTM15+ bathymetry grid [*Tozer et al.*, 2019]. Also shown as fine lines are tracks from cruises MGL-1309 [*Martinez and Hey*, 2017] and KN189-04 [*Hey et al.*, 2010]. Evenly spaced fine lines are plate spreading flowlines from *Smallwood and White* [2002]. The *R/V Neil Armstrong* flowline-oriented tracks were designed to span the change in opening direction on the ridge flanks and join with flowline tracks from the previous cruises, extending the coverage to the Reykjanes Ridge axis. The survey also maps the Bight Triple Junction at the southwest corner of the survey, follows along the Bight Fracture Zone, expands on the coverage of the first spreading segment south of the Bight Fracture Zone and conducts a shorter series of flowline profiles on the conjugate eastern flank of the ridge.

The tectonic reorganizations of the Reykjanes Ridge have been viewed in terms of two broad classes of models. In one class of models, a dynamically changing mantle plume is proposed to affect the rheology of the North Atlantic lithosphere by regionally changing the underlying mantle temperature, so that under "hot" mantle conditions the lithosphere behaves in

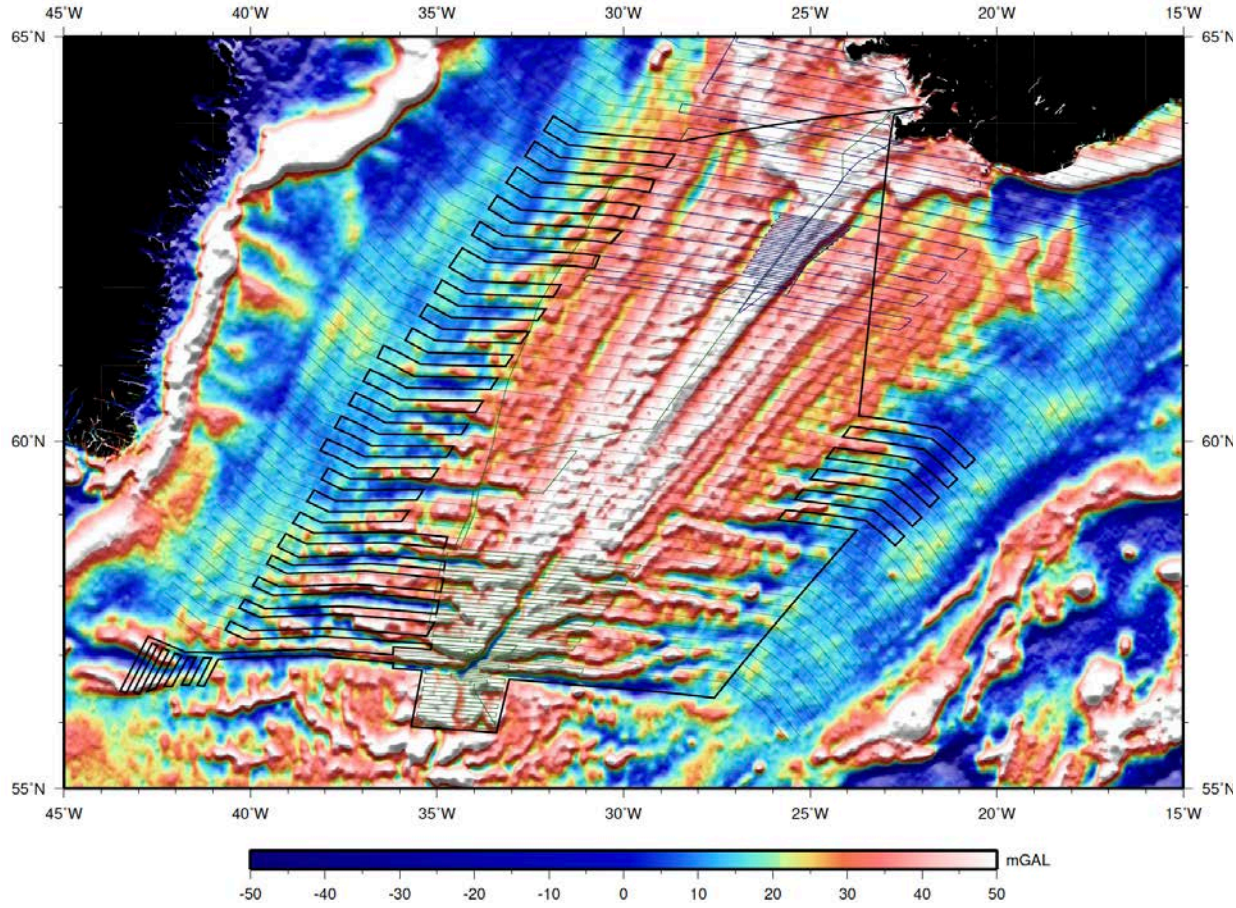

Figure 4) Survey track overlaid on satellite-derived free air gravity anomalies [*Sandwell et al.*, 2014]. The free air gravity map delineates basement structure on the ridge flanks better than topography (Fig. 3) due to its density contrast with blanketing sediments. The survey is designed to span the interval before the fracture zones formed to after their development and link to two previous surveys that map their subsequent evolution and elimination. Other features as in Fig. 3.

a ductile manner and "brittle" features such as transform faults cannot from while at other times decreased mantle plume influence or temperature leads to stronger lithosphere allowing formation of transform faults [*Abelson et al.*, 2008; *Jones*, 2003; *White*, 1997]. These models also predict changing crustal thicknesses as a result of changing mantle temperature beneath the ridge axis. In the other class of models, kinematic and plate boundary processes control the tectonic evolution of the Reykjanes Ridge. Lithospheric processes such as ridge propagation, asymmetric spreading, migrating non-transform discontinuities and as well as seafloor spreading melting regime processes such as migrating buoyant mantle upwelling instabilities are the mechanisms that control the tectonic reorganizations [*Benediktsdóttir et al.*, 2012; *Benediktsdóttir et al.*, 2016; *Hey et al.*, 2010; *Hey et al.*, 2016; *Martinez and Hey*, 2017]. Crustal thickness changes result from ridge segmentation itself through its direct effects on mantle upwelling and melting [*Magde and Sparks*, 1997; *Phipps Morgan and Forsyth*, 1988] with no change in mantle temperature needed. In these models the regional mantle anomaly (the hotspot) itself is a relatively passive feature, affecting the plate boundary processes primarily through its

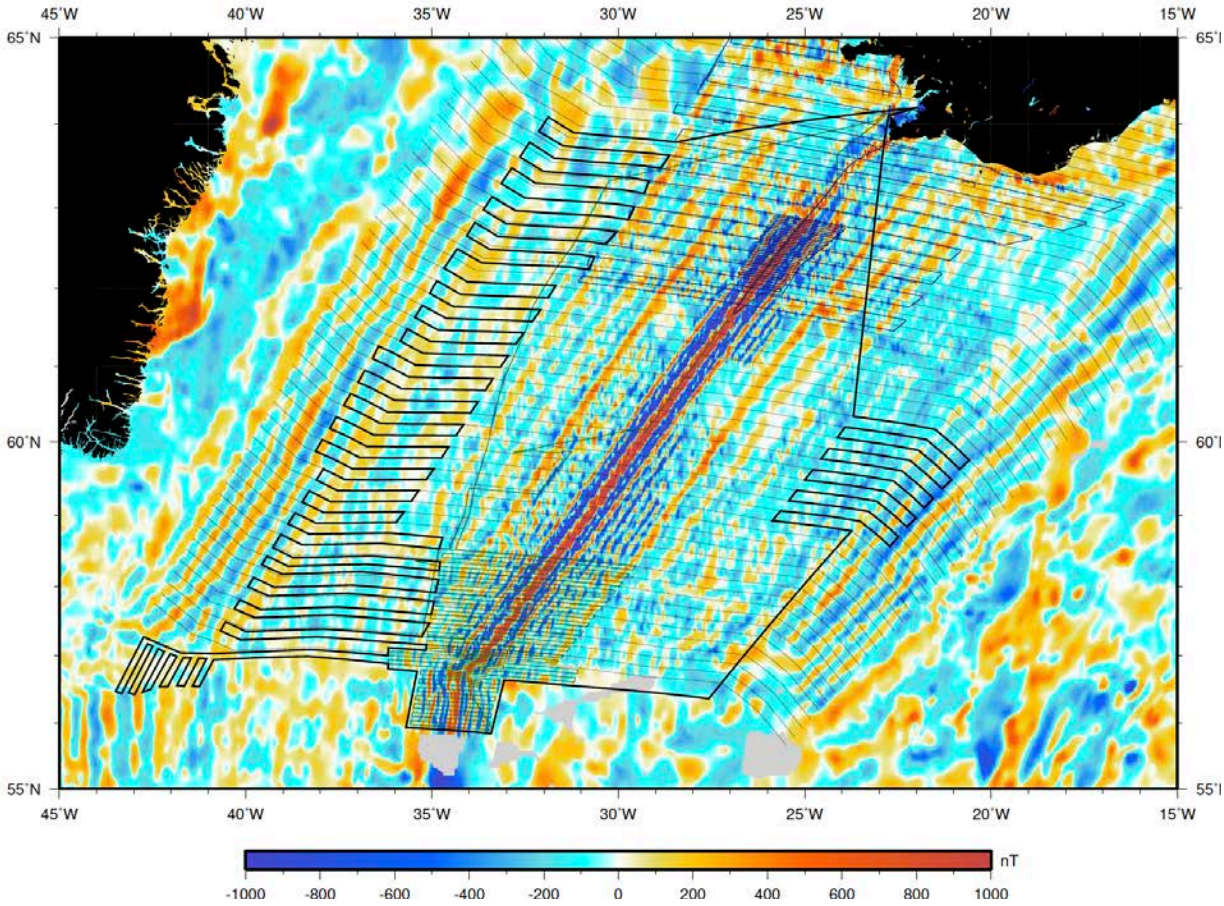

Figure 5. Survey track overlaid on compiled magnetic anomaly grid [*Macnab et al.*, 1995] with additional ship magnetic data added in near-axis areas from *R/V Knorr, Langseth* and *RRS Charles Darwin* cruises (see text). The regional magnetic anomaly map broadly delineates the transition from a linear ridge to a stair-step segmented ridge and back to a linear ridge but has too coarse a resolution to identify the processes involved. High-resolution flowline profiles will allow a much finer determination of the kinematics involved. Note the much higher resolution in areas of the near-axis surveys. Other features as in Fig. 3.

persistent regional gradient in melting properties with distance from Iceland and no dynamic mantle changes are implied to cause the tectonic reorganizations.

In order to address these issues a 36-day geophysical survey (24 June to 29 July, 2019) was conducted on *R/V Neil Armstrong* operated by the Woods Hole Oceanographic Institution. The survey was designed to obtain new geophysical data that bear on the timing and geologic mechanisms that effected the reconfigurations. Generalized mechanisms involving brittle to ductile lithospheric transitions had been previously inferred primarily from regional satellite-derived gravity maps (e.g., Fig. 4) and gridded low-resolution magnetic anomaly compilations (e.g., Fig. 5). By better understanding the kinematics and geologic mechanisms effecting the tectonic reconfigurations, discrimination can be made between plate boundary processes and alternative thermally-induced ductile/brittle lithospheric transformations and thus test these models. The objectives of the cruise were therefore to acquire a set of coincident bathymetric, potential field and sediment echosounder profiles navigated along seafloor spreading flowlines that would determine the detailed kinematics of the reconfigurations (through identifying

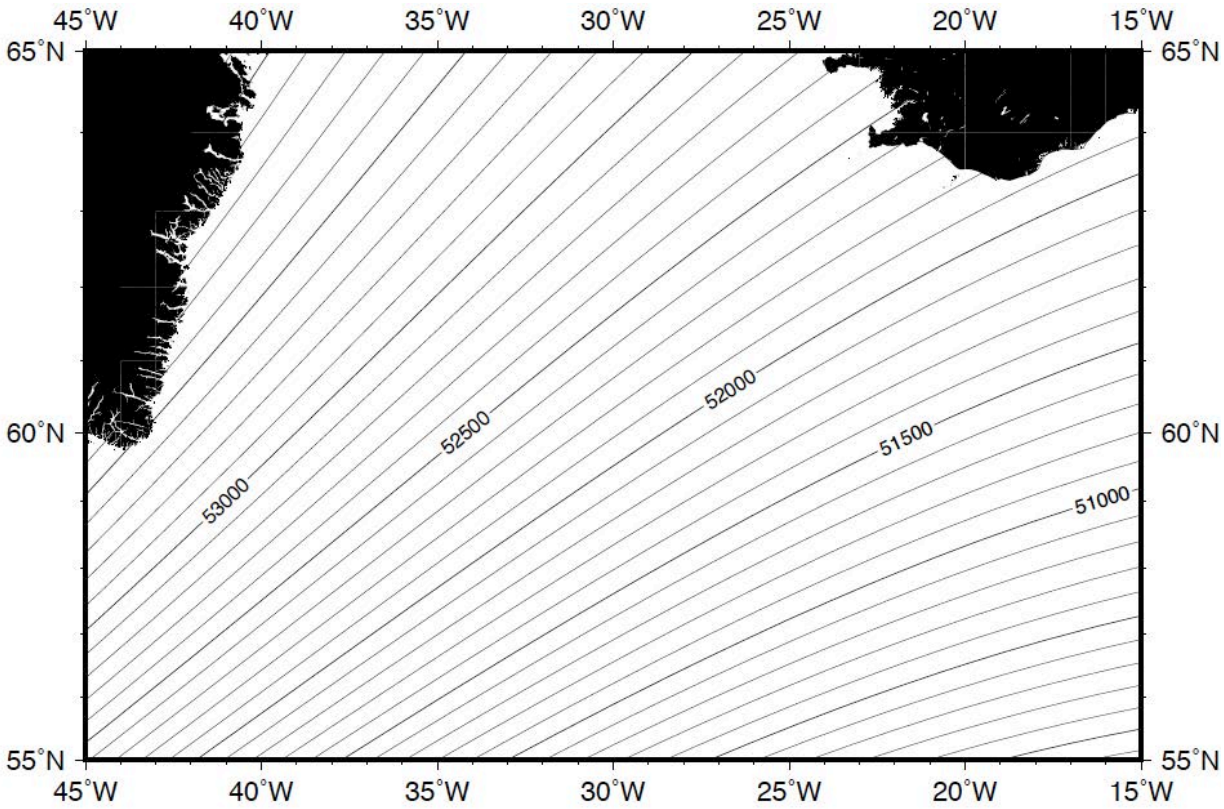

Figure 6. Map of the total magnetic field variation in nT in the survey area calculated from the IGRF for mid-July 2019 from https://www.ngdc.noaa.gov/geomag/calculators/magcalc.shtml#igrfgrid. Contour interval is 100 nT.

magnetic isochrons), tectonic structure (through direct mapping of basement exposures and gravity modeling of buried structure) and assess relative crustal thickness changes (through gravity modeling) that that can constrain mantle thermal changes [*White*, 1997] or be explained by effects of plate boundary segmentation on mantle upwelling without mantle thermal changes [*Magde and Sparks*, 1997; *Phipps Morgan and Forsyth*, 1988].

The survey acquired total magnetic intensity (with a Sea Spy Overhauser-type magnetometer) and gravity (with a Bell BGM-3 accelerometer-type gravimeter) measurements along with 3.5 kHz sediment echosounder (Knudsen 3620) profiles and multibeam (Kongsberg-Simrad EM122 and EM710) bathymetry and acoustic backscatter data. The underway survey of the fracture zone terrain was navigated along seafloor spreading flowlines following the Euler stage poles of *Smallwood and White* [2002]. Unlike most previous surveys in the area, flowline profiles relate ridge flank observations along the profile to their nominal single origin position on the ridge axis. This is especially important where there are systematic gradients in observed quantities along the ridge, as at the Reykjanes Ridge, where along-axis distance from the Iceland hotspot is an important variable affecting melting, crustal thickness and depth. Although the transient fragmentation of the Reykjanes Ridge axis into offset stair-step segments introduces complications into the interpretation of flowline profiles, such profiles nevertheless minimize effects of hotspot distance and facilitate the identification of ridge jumps, rift propagation, asymmetric spreading and migration of non-transform discontinuities.

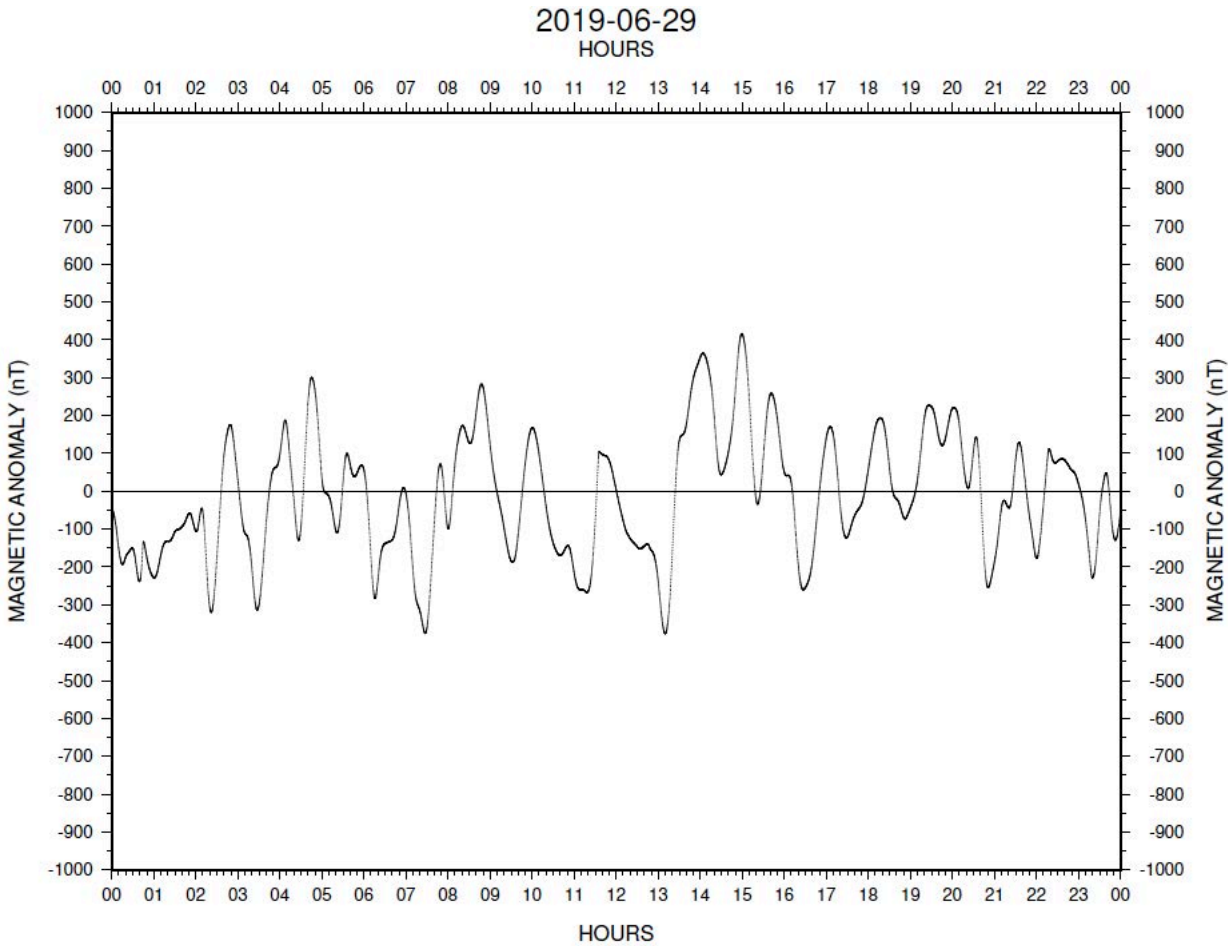

Figure 7. Example daily plot of the total field magnetic anomaly (IGRF removed) used to assess data acquisition and quality.

The survey plan was divided into several stages. First were a series of flowline profiles nominally between anomalies 20 and 8 spanning the change in opening direction with some of the profiles having their younger ends extended to match previous flowline tracks from *R/V Knorr* (KN189-04) [*Hey et al.*, 2010] and *R/V Langseth* (MGL-1309) [*Martinez and Hey*, 2017] cruises that spanned the ridge axis. This would allow extending magnetic isochron identifications continuously across the flanks to the ridge axis. Along-strike, the fracture zone flowline profiles cover the area from near the Iceland shelf to the Bight Fracture Zone and were intended to study how the plate boundary reorganization varied with distance along the "hotspot" mantle gradient south of Iceland (Figs. 3-5).

At the SW end of the fracture zone lines, a short survey of the extinct Bight Triple Junction (Fig. 3) followed. Before about anomaly 17 three spreading centers met at this triple junction: the Labrador Sea spreading center, the early Reykjanes Ridge, and the Mid-Atlantic Ridge [*Johnson et al.*, 1973; *Kristoffersen and Talwani*, 1977; *Laughton*, 1971; *Vogt and Avery*, 1974]. The extinction of the Labrador Sea spreading center resulted tectonically in Greenland joining to the North American plate and the Reykjanes Ridge becoming the new North America-Eurasia plate boundary [*Smallwood and White*, 2002]. The converging wedge-shaped elevated tectonic edges bounding the crust formed on the Labrador Sea spreading center delineate its

failed tip [*Johnson et al.*, 1973]. The failure of this ridge also appears to be related to the ~30° change in opening direction across the Reykjanes Ridge that led to the fragmentation of the axis into stair-step segments [*Smallwood and White*, 2002]. Because of the importance of this event in the tectonic development of the North Atlantic basin, the survey of this area was designed to better constrain the timing of triple junction failure, its tectonic characteristics and how its failure led to the conversion of the triple junction into the Bight Transform Fault as the Reykjanes Ridge transitioned from forming the Greenland-Eurasia plate boundary to the new North America-Eurasia plate boundary.

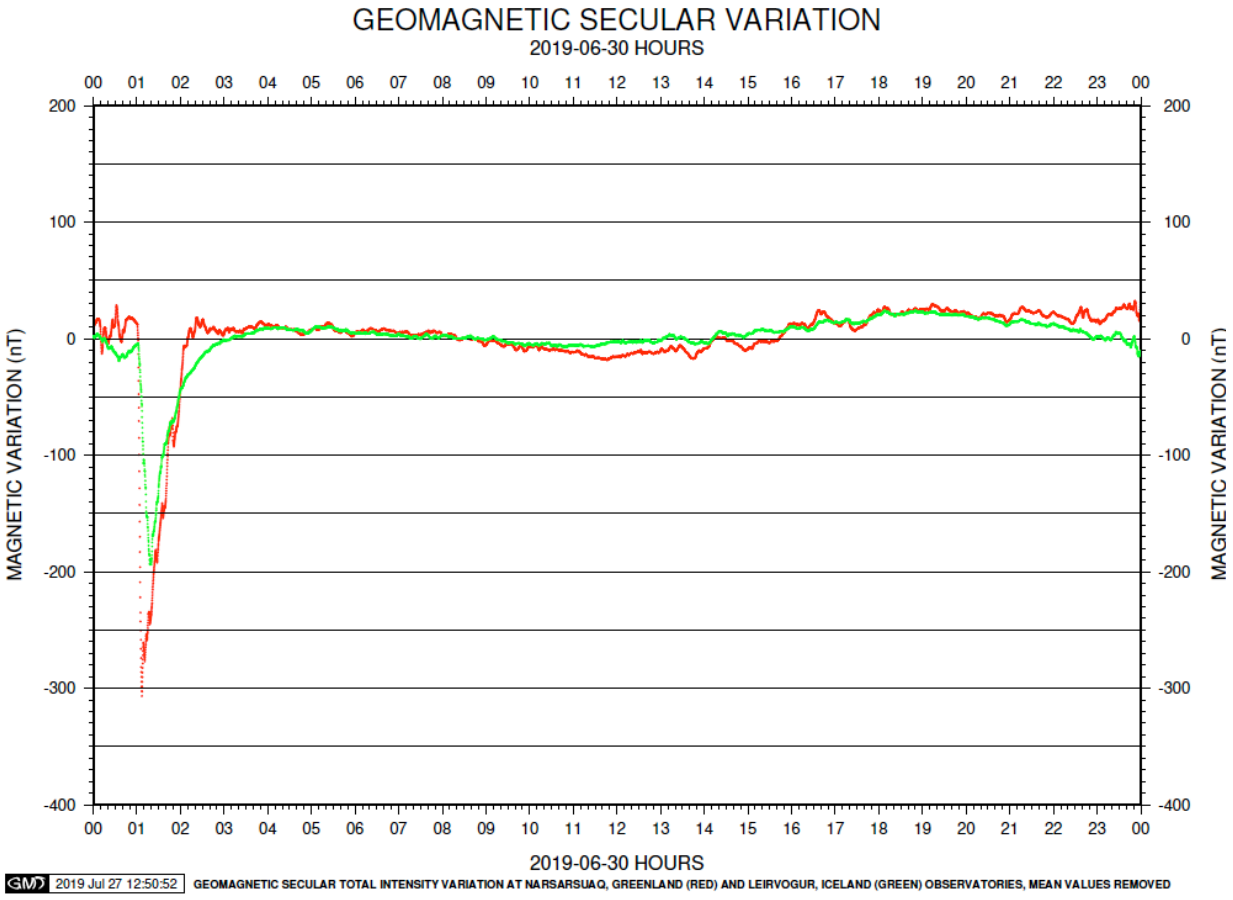

Figure 8. Example geomagnetic observatory data for assessing secular variation. The total field magnitude (intensity) was calculated from the horizontal and vertical vector components and the IGRF calculated using the GMT program *mgd77magref* and subtracted from the total field values. The mean of each profile was then subtracted from each respective profile. Plots show the intensity variations measured at the Leirvogur, Iceland (green dots) and the Narsarsuaq, Greenland (red dots) Geomagnetic Observatories. The similar shapes indicate that the secular variations are regional in extent, as these observatories span the survey area across the Irminger Basin, suggesting it is feasible to attempt a secular variation correction to the observed ship values.

The survey then follows the Bight Fracture Zone eastward in order to better determine its geometry. As noted above, the Bight Fracture Zone constrains North America-Eurasia opening following the failures of the Labrador Sea spreading center and the Bight Triple Junction. Thus, the tracks here aim to better delineate its geometry and thereby North America-Eurasia relative

plate motion during the time the segmented Reykjanes Ridge existed and evolved back to a linear configuration. Although sediments fill a great deal of the wide fracture zone valley, we found that in places narrow ridges rise through the sediments and accurately delineate the fracture zone trend. The close match of this flank fracture zone trend with that of the well-mapped presently active Bight transform fault [*Appelgate and Shor*, 1994; *Martinez and Hey*, 2017] indicates a stable opening direction during the time when the offset segments evolved back to a linear but obliquely-spreading Reykjanes Ridge axis.

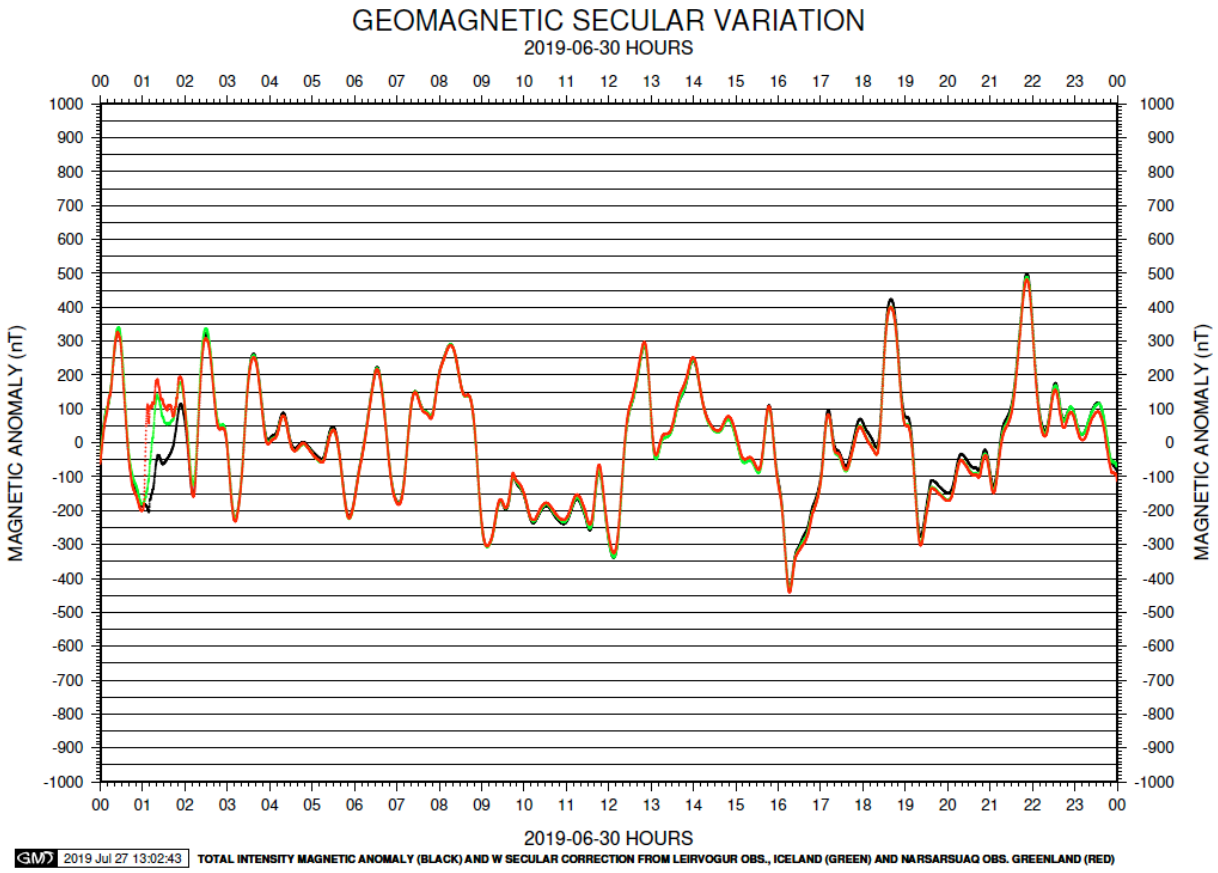

Figure 9. Test correction of magnetic anomaly data for secular variation. The curves show the original magnetic anomaly data (black dots) and the values corrected by subtracting the temporal variations observed at the Leirvogur, Iceland (green dots) and the Narsarsuaq, Greenland (red dots) Geomagnetic Observatories (Fig. 8). The large excursion measured at both observatories between about 01:00 and 02:00 hours (Fig. 8) has an appreciable effect on the shape of the total field anomaly ship measurements. Other secular variations are smaller and have a negligible effect on the overall magnetic anomaly shape of the ship measurements.

The eastern end of the Bight Fracture Zone track on the western ridge flank abuts the previous *R/V Marcus G. Langseth* survey of the first spreading segment south of the fracture zone. Our tracks thus follow along the perimeter of this previous survey in order to expand on the coverage and map the southern segment boundary, which was not achieved on the *Langseth* survey. This first segment south of the Bight Fracture Zone is important because of its contrasting characteristics with the Reykjanes Ridge north of the Bight transform fault [*Appelgate and Shor*, 1994; *Benediktsdóttir et al.*, 2016; *Martinez and Hey*, 2017]. This segment

has geologic and geophysical characteristics more typical of orthogonally-spreading Mid-Atlantic Ridge segments to the south compared to the obliquely-spreading Reykjanes Ridge. It thus serves as a tectonic, geologic and geophysical reference along the same plate boundary for comparisons with the Reykjanes Ridge.

The survey then continues along the eastern Bight Fracture Zone to its intersection with the location of the change in plate motion, nominally near anomaly 17. Thus, the Bight Fracture Zone survey of the eastern flank will also help delineate its geometry and properties through its gravity signature, since sedimentation is greater on the eastern flank and masks its tectonic expression in bathymetry.

On reaching the nominal position of anomaly 17 [*Smallwood and White*, 2002], the track follows this isochron to the NE. If the ridge segmentation abruptly formed at this time it may be possible to detect the segmented crust in the gravity data and through magnetic anomalies, despite the nearly complete sediment drape. Our track then resumes a series of flowline profiles conjugate to a set on the western flank. The flowline profiles here also bracket the change in spreading direction and are additionally intended to investigate a significant asymmetry in the regional magnetic anomaly pattern. The band of positive magnetic anomalies near 17 is appreciably wider on the western ridge flank compared to its conjugate on the eastern ridge flank, as mapped in a regional data compilation (Fig. 5) [*Macnab et al.*, 1995]. By surveying both conjugate flanks we hope to determine the tectonic cause of the asymmetry, which appears to be a general feature of the mechanism by which the originally linear axis became fragmented into a stair-step array of segments. Several general geologic and conceptual mechanisms have been proposed for this type of tectonic reconfiguration [*Hey et al.*, 1988; *Menard and Atwater*, 1968] and the reverse process of eliminating segment offsets [*Vogt and Johnson*, 1975] and our survey of the conjugate flanks is intended to provide the data to resolve the mechanism. On completing these flowline-oriented profiles, we sailed back to Reykjavik using the transit to survey near the ridge axis to complete the cruise (Fig. 1).

Data Acquisition:

The *R/V Neil Armstrong* departed Reykjavik Harbor on 24 June 2019 at 10:00 (UTC). After clearing the harbor and coastal areas we deployed the magnetometer at 15:00 and began collecting the full set of underway data. Our nominal survey speed was 10 knots but varied due to weather conditions. The planned ship track is shown in Figures 3-5 overlaid on SRTM-15 topography [*Tozer et al.*, 2019] (Fig. 3), satellite-derived gravity [*Sandwell et al.*, 2014] (Fig. 4) and compiled magnetic anomaly grids [*Macnab et al.*, 1995] supplemented with ship magnetic data primarily from R/Vs *Knorr* [*Hey et al.*, 2010], *Langseth* [*Martinez and Hey*, 2017] and *RRS Charles Darwin* [*Searle et al.*, 1998] (Fig. 5) surveys. The survey acquired a continuous and coincident array of underway data including Kongsberg-Simrad EM122 multibeam bathymetry, supplemented in shallow areas by EM710 data, total-field magnetic intensity measurements made with a SeaSpy Overhauser-type magnetometer, Gravity measurements made with with a Bell BGM-3 gravimeter, and sediment profiler records made with with a Knudsen 3620 echosounder operated at a central frequency of 3.5 kHz. To provide water column sound velocity information for the multibeam system, temperature-depth profiles were obtained with expendable bathythermographs (XBTs) on an approximately daily basis. The XBT measurements were distributed such as to more or less evenly sample the survey area. A few T5 but mostly T7 and Deep Blue XBT models were used that could be deployed at full survey

speed, as the T5's required the ship to slow to 6 knots or less for deployment, affecting the gravity measurements. No offsets or changes in character of the multibeam data were noted with entry of new XBT profile data into the multibeam system and data quality remained good except for weather-induced issues.

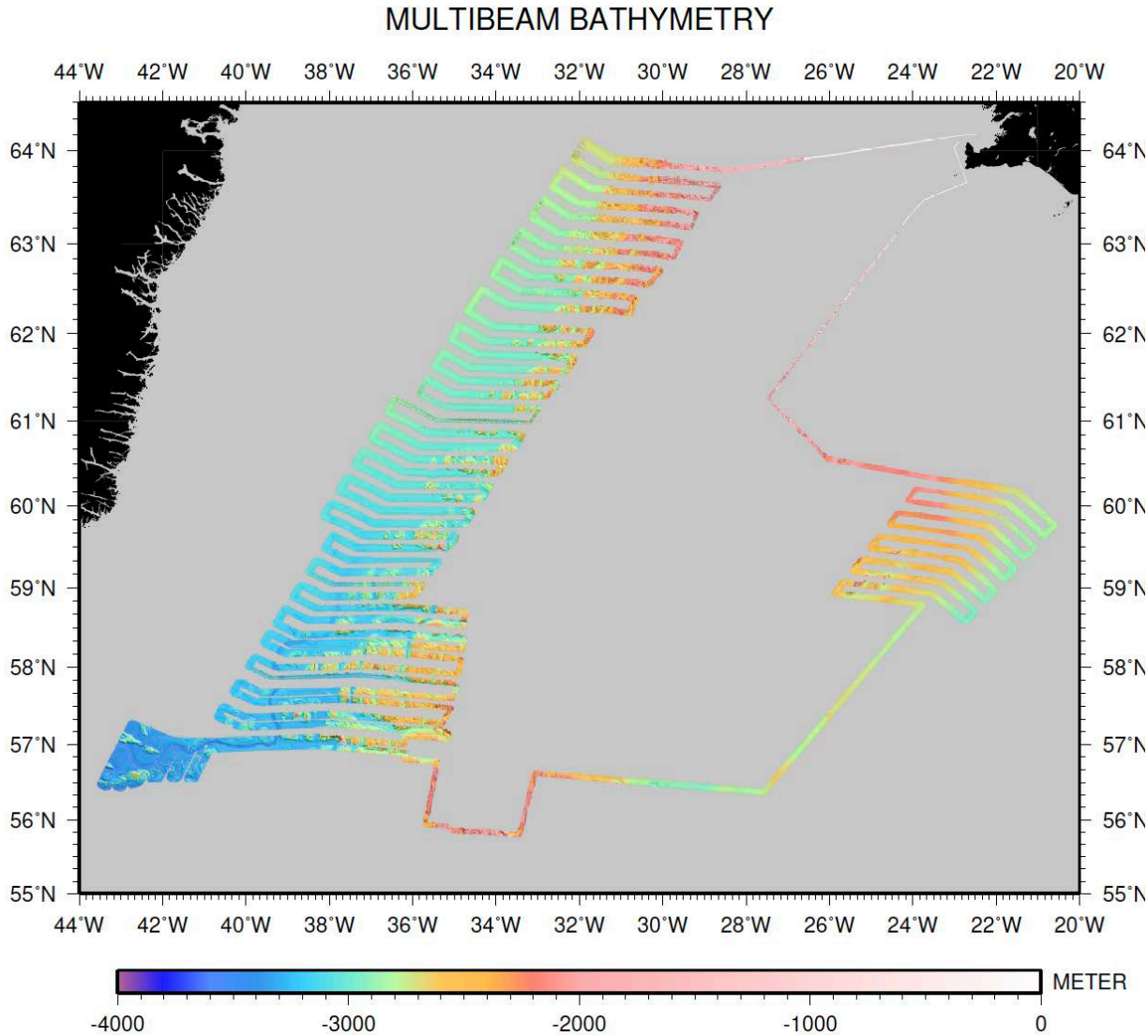

Figure 10. Full multibeam grid processed with MB-System and GMT software to provide first-pass cleaned data for rapid daily viewing at sea to assess data quality and coverage. Finer scale cleaning and processing was carried out with Caris software. A total area of 130,507 km² was mapped with the combined EM122 and EM710 multibeam systems.

Multibeam System:

The Simrad-Kongsberg EM122 multibeam system was operated throughout the cruise acquiring both bathymetry and acoustic backscatter data. EM710 data were also acquired in shallow (mostly <1000 m) areas at the beginning and end of the cruise. A total area of 130,507 km^2 was mapped. Water column data from the multibeam systems were also recorded. For the most part, the beam angular coverage was set to automatic selection with a maximum of 75° on each side

except during times of bad weather when coverage was narrowed since outer beams were consistently lost under these conditions. The multibeam data were processed onboard using a combination of Caris Software and MB-System and GMT software. The MB-System and GMT software were used to produce plots that could be cleaned and gridded routinely quickly to assess data quality, coverage and make preliminary geologic interpretations. Finer scale data cleaning and rendering was accomplished with the Caris software.

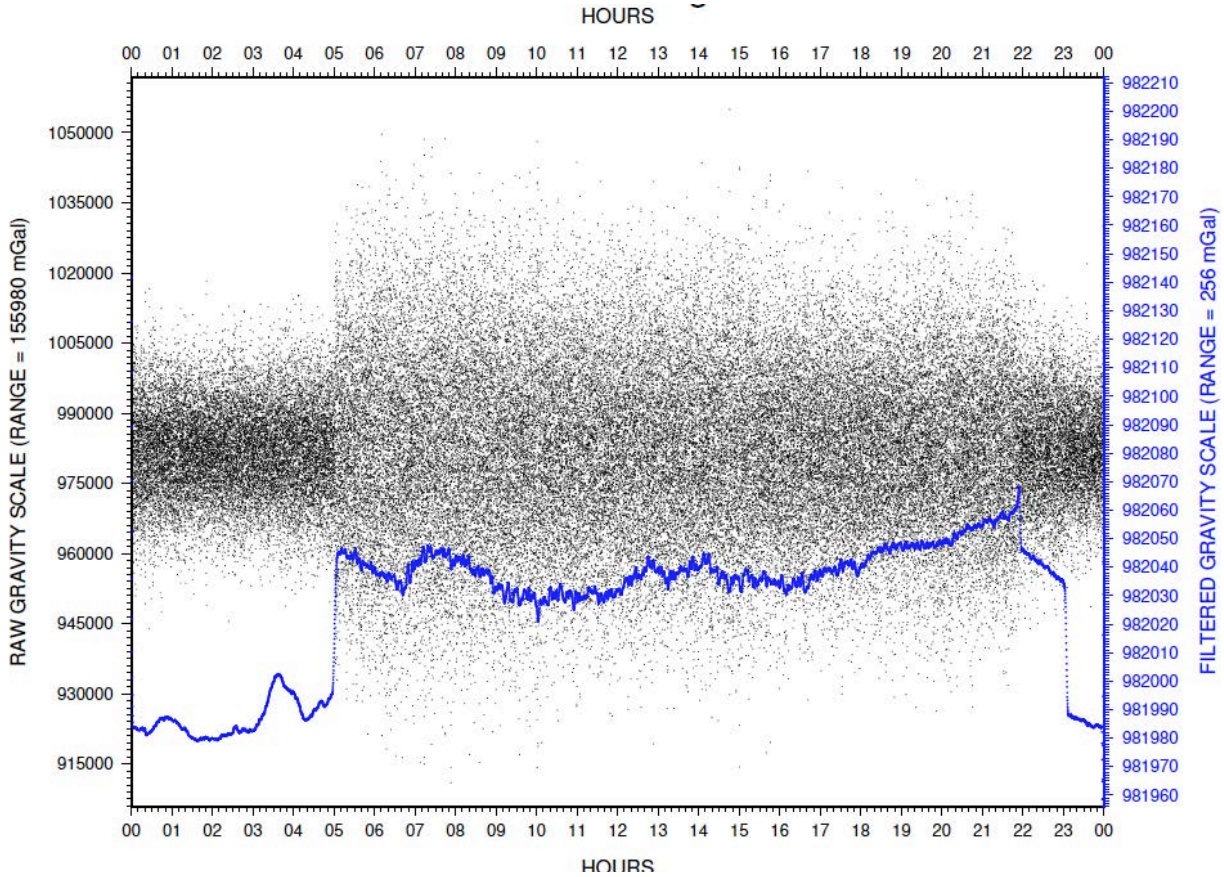

Figure 11. Example daily plot of the raw BGM-3 gravity data (fine black dots) and 300 second cosine tapered filtered gravity (blue dots) illustrating how the short-duration accelerations (primarily due to waves and swells) average to essentially zero over this time, revealing longer duration accelerations. Abrupt step-like jumps are due to course and/or speed changes, which are later removed in the Eötvös correction.

For the most part, erroneous beams tend to form outliers far off the actual depth. We take advantage of this property to remove outliers in an automated script and make gridded maps of the multibeam data that can be updated quickly. We use the MB-System program *mblist* to extract longitude, latitude, topography triplets for each ping and compare the data to a reference topography surface (SRTM-15+ [*Tozer et al.*, 2019]). Using the UNIX utility *awk* we then exclude data point more than 1000 m above or more than 700 m below this reference surface. This produces a set of data files that have been culled to exclude these outliers. These culled values are then gridded using the GMT program *xyz2grd* at 0.001x0.001 degree cells (roughly 50x100 m in the survey area). Small gaps in this grid are filled by running a 0.005x0.005 boxcar filter over the data using the GMT program *grdfilter*. The original grid of culled values is then superimposed on this filtered grid using the GMT program *grdmath* with the AND operator. The

resulting grid has no loss in resolution compared to the culled grid but has small gaps filled by interpolation from surrounding cells that have data. A gradient grid is then made using the GMT program *grdgradient* and a plot made of the illuminated bathymetry using the GMT program *grdimage*. A plot of the bathymetry grid image is shown in Figure 10.

Data quality was good to poor depending on the sea conditions. Waves above 2 m often resulted in poor multibeam quality likely due to sweep down of air bubbles beneath the hull-mounted transducers. Approximately 8500 trackline nautical miles (15,742 km) of bathymetry and water column data were collected. The raw multibeam data were logged in approximately half hour-long files in the Kongsberg Simrad EM122 raw format (*.ALL and *.WCD). Data files contain, sound velocity profile information, navigation, backscateter, Roll-Pitch-Yawn, TWT. The MB-System 5 software package or Caris HIPS Version 11.0.8 © was be used to access the files and do fine beam editing of the files.

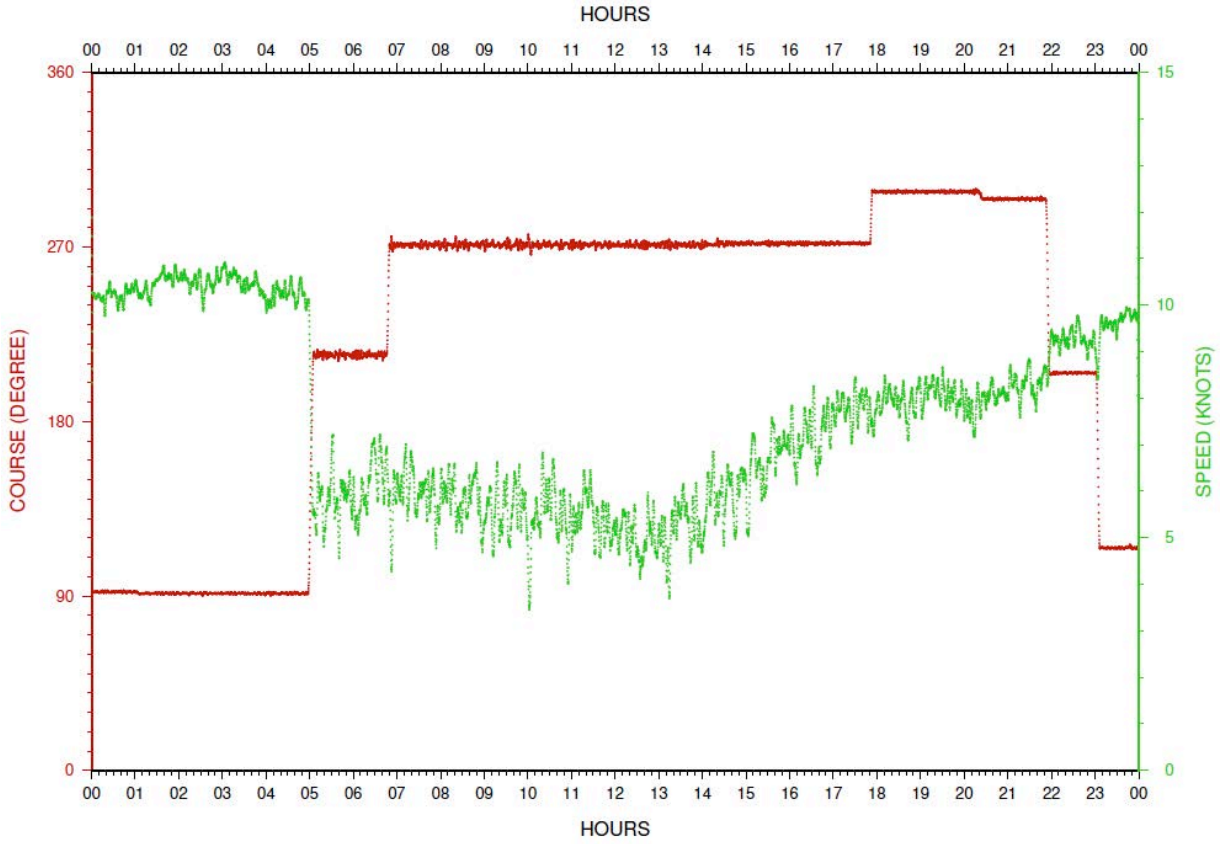

Figure 12. Example daily plot of course (red dots) and speed in knots (green dots) for use in the Eötvös correction to the gravity data.

The logged Multibeam data files were transferred from the data acquisition computer to data storage and the Caris Software processing machine. All data files were edited while at sea using the Caris HIPS processing system (Version 11.0.8). Armann Hoskuldsson and Daniel Þorhallsson supervised the editing and supervised other science party members editing the bad data points outside the valid depth range for each hour of data. When the data were judged acceptable, the data was gridded in Caris and then exported as XYZ (longitude, latitude, depth) files. These files are then usable in any geographic information software. At the end of the cruise, the data was copied to a portable hard drive.

Speed of Sound Corrections The travel time of sound in water measured at the transducer and supplied directly to the EM122 system serial port and the data was transmitted by the RVDAS program rv_tsg. Water column sound velocity profiles were calculated from XBT casts on approximately a daily basis but we attempted to distribute the XBTs approximately evenly within the survey area. No noticeable change in the processed swath bathymetry was discernable with new XBT profiles applied to underway data.

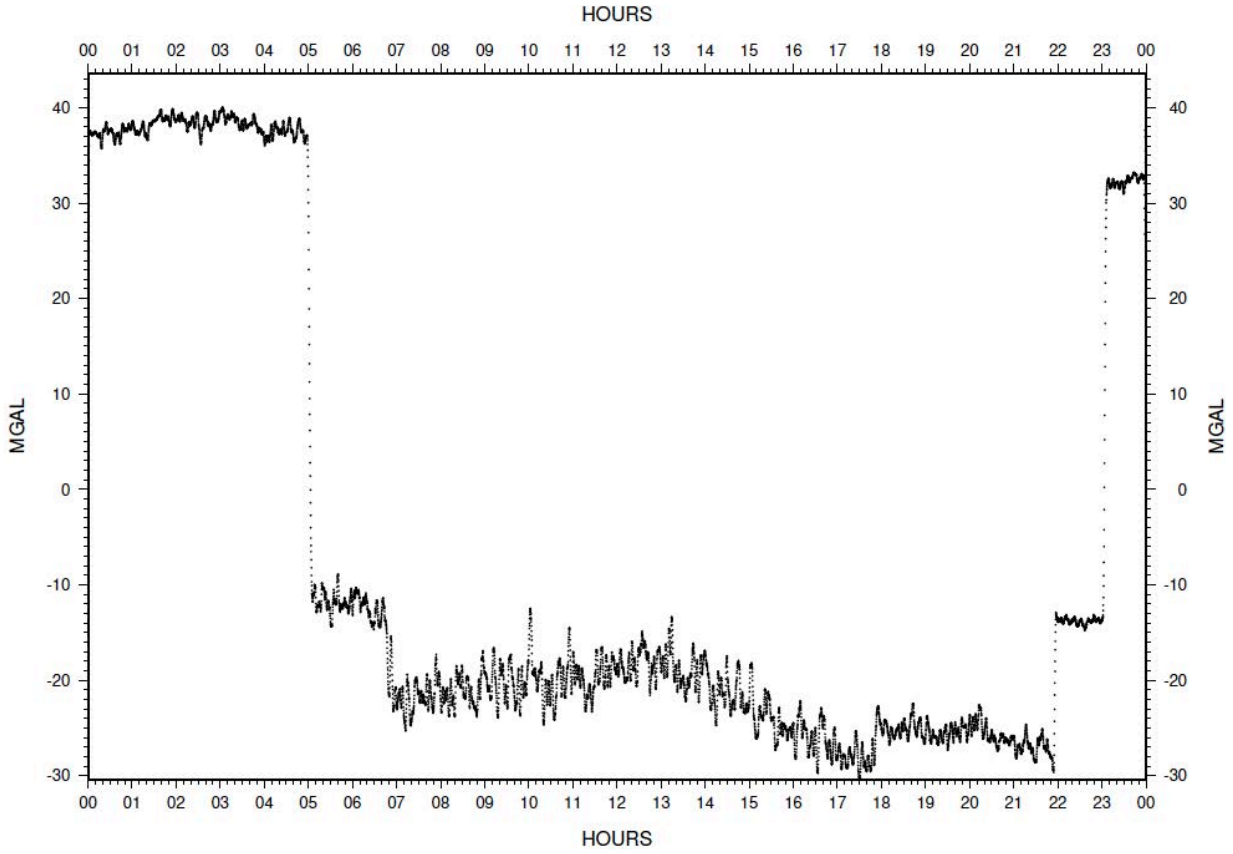

Figure 13. Example daily plot of the Eötvös gravity correction for ship course and speed at a particular latitude.

Magnetic Data

Total field magnetic data were recorded with a *SeaSpy* Overhasuser-type magnetometer towed at a distance of 333 m behind the ship, estimated from the nominal deployed length of cable plus the distance from the magnetometer winch to the GPS antenna. The *SeaSpy* "BOB" software calculated a layback corrected position relative to the GPS antenna for each magnetometer measurement. Raw data recording was set to one Hz. The magnetic anomaly was then calculated by using the GMT program *mgd77magref,* which calculated the International Geomagnetic Reference Field (IGRF) value valid for 2015-2020 for each total field position and time. The IGRF values were then subtracted from the total field measurements to yield the magnetic anomaly. A contour map of the IGRF values for the survey region is shown in Fig. 6. The magnetometer time series was then median filtered and output at 10 second intervals using the GMT program *filter1d*. Plots of the magnetic anomaly vs. time (e.g. Fig. 7) were reviewed daily for assessing data quality. On July 12 the magnetics logging program developed

synchronization errors that resulted in data gaps up to about an hour in duration. After consulting with the manufacturer and shore-based technical team it was decided to swap out the transceiver box and GPS com port cable and clean the water-tight connectors between the winch and the magnetometer cable. The data acquisition program and logging system were also restarted as a new survey. This combination of actions resolved the problem with the synchronization errors and data were acquired normally thereafter.

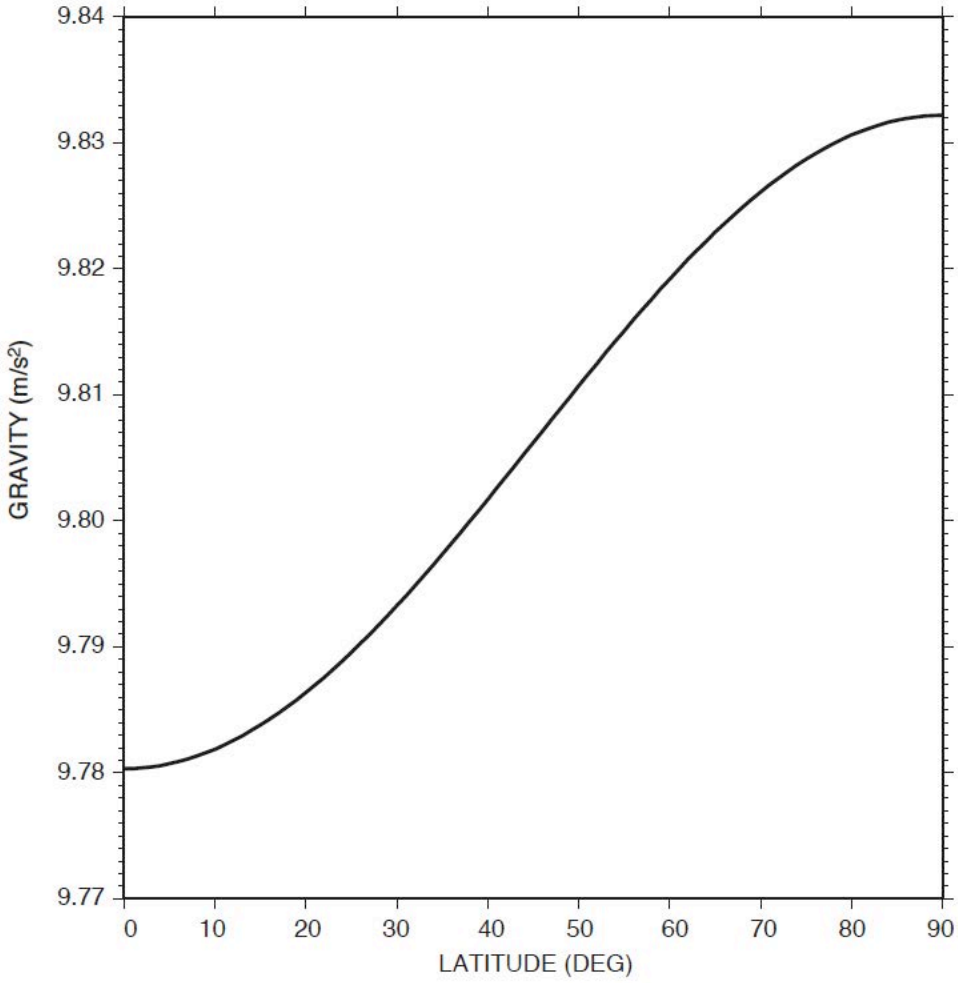

Figure 14. International Gravity Formula:
978032.53359 × (1+0.00193185265241*sin²(α))/sqrt(1-0.00669437999013*sin²(α))
in mGals for the Earth's gravity variation with latitude (α) using ellipsoid parameters for WGS84. Plot shows gravity values in m/s².

Because secular geomagnetic variations can be significant, in particular at high latitudes, we downloaded available time series data covering part of the cruise from the Leirvogur, Iceland and the Narsarsuaq, Greenland Magnetic Observatories to monitor secular variations during the cruise. An example of one of the larger variations is shown in Fig. 8. Examining data over several days indicated that the larger secular variations measured at these observatories is regional in extent and may therefore be used to remove these variations from the measured magnetometer data (Figs. 8 & 9). Post cruise we will investigate if the effect can be removed from the entire cruise magnetic time series using data from additional observatories.

In addition to plotting the daily magnetic anomaly time series to monitor data quality, profiles of the magnetic anomaly vs. distance along the profile were made. Such profiles will be used to identify magnetic isochrons by forward calculating the magnetic anomaly from the geomagnetic reversal sequence and making visual correlations of the reversal patterns. Since the profiles were acquired along estimated spreading flowlines [*Smallwood and White*, 2002] no projection into the spreading direction is necessary.

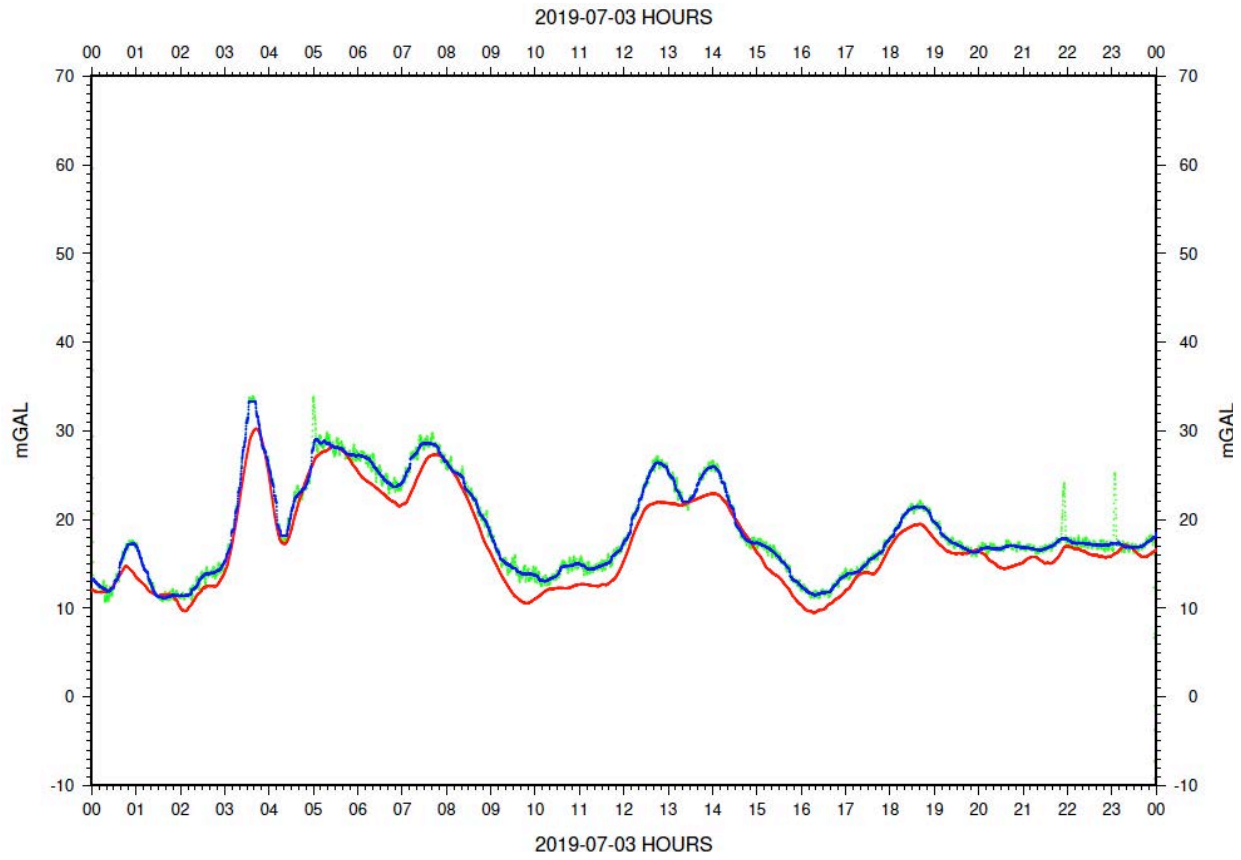

Figure 15. Example daily plot of the free air gravity anomaly (blue line) after applying median filter to remove spikes caused by course and/or speed changes and other jitter introduced by the Eövös correction applied to the gravity values (green curve). Also shown for reference is the satellite-derived free-air gravity anomaly (red line, [*Sandwell et al.*, 2014]) sampled at the same locations as the ship gravity.

Gravity data

Gravity data were acquired using a Bell Aerospace BGM-3 gravity meter (S/N 220) mounted on a gyro-stabilized platform that maintained the accelerometer axis in a vertical orientation. A description of the meter and typical operating procedures are given in [*Bell and Watts*, 1986]. A dock-side gravity tie with a known absolute gravity datum was made prior to departing Reykjavik and on return to the same pier. Gravity values were also recorded by the BGM-3 gravimeter for at least a day while docked before and after the cruise to further calibrate

the gravimeter and assess drift (Fig. 16). The *R/V Neil Armstrong* was moored at the Grandagardur Pier, first at the SE end of the pier (64.15374°N, 21.94033°W) and on return at the NE side (64.15446°N, 21.93998°W). Both locations are within 100 m of reference gravity station #0100.04 with a datum value of 982,266.77 mGal located at 64.154167°N, 21.941667W.

The BGM-3 gravimeter records values in meter "counts" that are converted to mGal units with a calibrated scale factor for each meter (4.996899149). A "bias" value (855846.540) is then applied which yields the calibration tie gravity value determined pier side. A 300 second cosine taper filter was then applied to the gravity time series to remove the short-period vertical accelerations experienced by the ship.

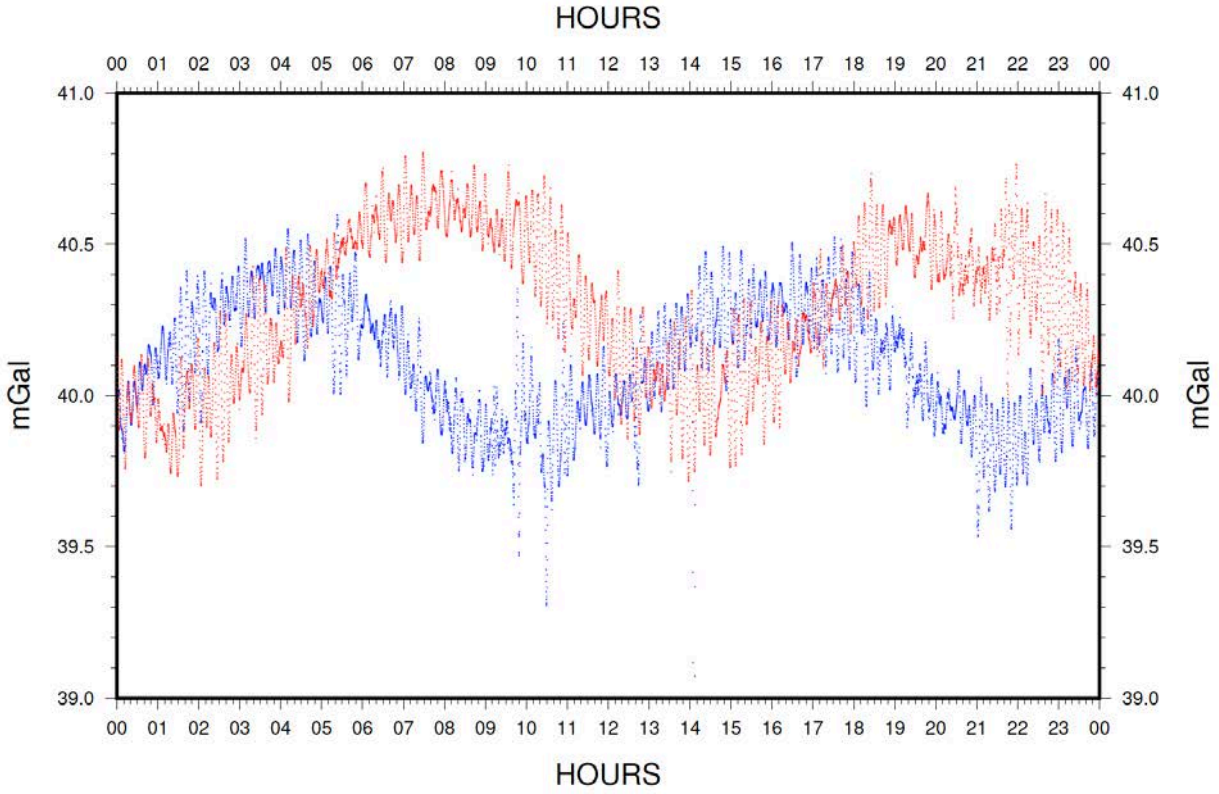

Figure 16. Free air gravity variations recorded by the ship's BGM-3 gravity meter while moored at the Grandagardur Pier over 24-hour periods before (blue) and after (red) the cruise. The moored variations are consistent with tidally-induced changes in ship elevation. Average gravity values over these 24-hour time periods are 40.1 and 40.3 mGals respectively and indicate no significant overall drift over the 36-day period of the cruise, given the short-term scatter of data and other uncertainties such as measuring ship elevations between fueling and loading events.

The filtered gravity then has the Eötvös correction applied which removes the accelerations due to ship course and speed at a particular latitude: $E = 7.503\ V \cos\phi \sin\alpha + 0.004154\ V^2$ where E is the Eötvös correction in mGal, V is the ship speed in knots, ϕ is the latitude in degrees, and α is the ship's course in degrees (azimuth) [e.g., *Glicken*, 1962]. Finally, the main variation in Earth's gravity due to latitude (the International Gravity Formula, Fig. 14) is removed from each value to yield the free air anomaly. The free air anomaly thus calculated retained some jitter and outliers introduced in part from short-term variations in ship speed and course changes (Fig. 12) not fully accounted for in the Eötvös correction [*Bell and Watts*, 1986].

After some experimentation we found that a 900 second median filter applied to the free air gravity values effectively removed this jitter and outliers at course changes without overly smoothing the signal (Fig. 15).

Knudsen sediment profiler

The Knudsen chirp echosounder was operated at a central frequency of 3.5 kHz throughout the cruise. Data was recorded in SegY format. The penetration varied from essentially none where only a hard seafloor return was produced to about 100 m where layered strata were evident. Although a variety deep-water flow features were evident in the Knudsen profiles, such as channels, sediment waves, and dunes our primary interest was in detecting sub-sediment basement and possible volcanic or tectonic sedimentary disturbances such as intrusions or faulting within the fracture zone terrain. At sea, the Knudsen profiles were monitored in real time on the system display and recorded files were further examined using Kogeo Seismic Toolkit 2.7. An example of the Knudsen sediment profiler data is shown in Fig. 16.

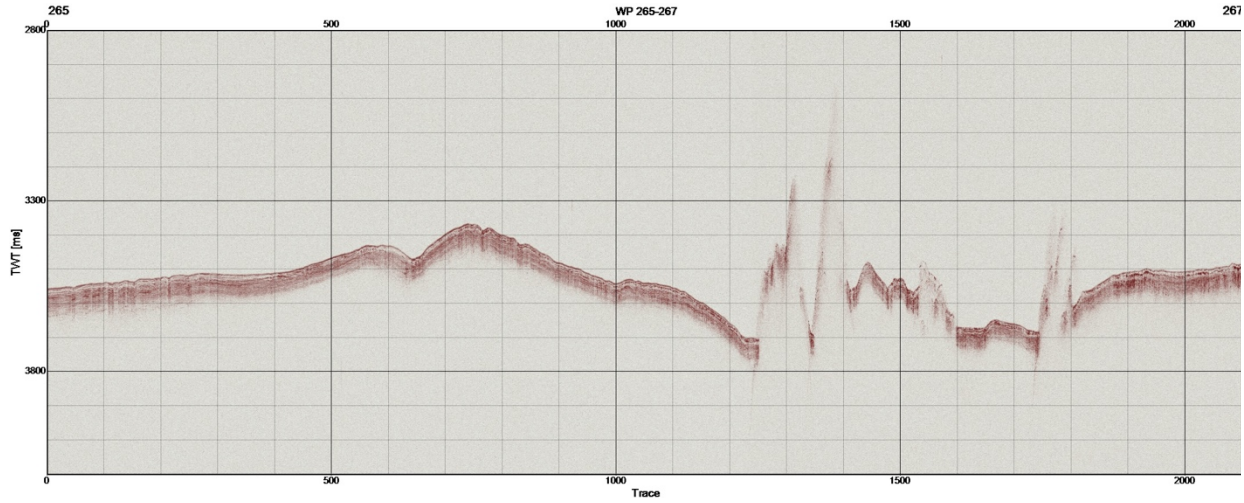

Figure 16. Example Knudsen 3.5 kHz sediment profile imaged in Kogeo Seismic Toolkit 2.7

Summary

All of the major objectives of the cruise were met. The survey covered the entire planned route obtaining coincident multibeam swaths, magnetic and gravity measurements and sediment echosounder profiles. Multibeam swaths were seriously degraded by weather conditions for only a total of little less than a day, primarily on July 3, 2019. Magnetic data gaps also were small totaling about two hours and occurring primarily on July 3 and July 12, 2019. Gravity values were obtained continuously with no gaps other than the typical expected excursions at course and speed changes. Sediment echosounder profiles were also continuous but were degraded during the same intervals as the multibeam bathymetry due to weather conditions. Variable penetration depended on sediment type. The survey data provide a modern, high-precision data set navigated primarily along seafloor spreading flowlines for assessing the tectonic evolution of the Reykjanes Ridge flanks and studying controls on the formation of ridge segments, transform faults and fracture zones and their evolution within a strong gradient in mantle melting properties.

Acknowledgements

We thank the Captain and crew of *R/V Neil Armstrong*, the Marine Technicians and the Science Party for their diligence and professionalism which contributed to the success of the scientific expedition. We also thank the governments of Iceland and Greenland for permission to work in their waters.

This work was funded by NSF grant OCE-1756760. The Marine Advanced Technology and Education program supported the participation of the MATE interns. An InterRidge Cruise Bursary supported the participation of Dr. Dominik Palgan.

References Cited

Abelson, M., A. Agnon, and A. Almogi-Labin (2008), Indications for control of the Iceland plume on the Eocene–Oligocene "greenhouse–icehouse" climate transition, *Earth and Planetary Science Letters*, *265*(1–2), 33-48, doi:http://dx.doi.org/10.1016/j.epsl.2007.09.021.

Appelgate, B., and A. N. Shor (1994), The northern Mid-Atlantic and Reykjanes Ridges: Spreading center morphology between 55°50'N and 63°00'N, *Journal of Geophysical Research: Solid Earth*, *99*(B9), 17,935-917,956.

Bell, R. E., and A. B. Watts (1986), Evaluation of the BGM-3 Sea Gravity Meter System Onboard R/V Conrad, *Geophysics*, *51*(7), 1480-1493, doi:Doi 10.1190/1.1442196.

Benediktsdóttir, Á., R. Hey, F. Martinez, and Á. Höskuldsson (2012), Detailed Tectonic Evolution of the Reykjanes Ridge During the Past 15 Ma, *Geochem. Geophys. Geosyst.*, *13*, Q02008, doi:02010.01029/02011GC003948.

Benediktsdóttir, Á., R. Hey, F. Martinez, and Á. Höskuldsson (2016), A new kinematic model of the Mid-Atlantic Ridge between 55°55'N and the Bight Transform Fault for the past 6 Ma, *Journal of Geophysical Research: Solid Earth*, *121*(2), 455-468, doi:10.1002/2015JB012504.

Glicken, M. (1962), Eötvös corrections for a moving gravity meter, *Geophysics*, *27*(4), 531-533.

Hey, R., F. Martinez, Á. Höskuldsson, and Á. Benediktsdóttir (2010), Propagating rift model for the V-shaped ridges south of Iceland, *Geochem. Geophys. Geosyst.*, *11*(3), Q03011.

Hey, R., F. Martinez, Á. Höskuldsson, D. E. Eason, J. D. Sleeper, S. Thordarson, Á. Benediktsdóttir, and S. Merkuryev (2016), Multibeam investigation of the active North Atlantic plate boundary reorganization tip, *Earth and Planetary Science Letters*, *435*, 115-123, doi: 110.1016/j.epsl.2015.1012.1019, doi:http://dx.doi.org/10.1016/j.epsl.2015.12.019.

Hey, R. N., H. W. Menard, T. M. Atwater, and D. W. Caress (1988), Changes in direction of seafloor spreading revisited, *Journal of Geophysical Research: Solid Earth*, *93*(B4), 2803-2811.

Johnson, G. L., J. Egloff, J. Campsie, M. Rasmussen, F. Dittmer, and J. Freitag (1973), Sediment distribution and crustal structure of the southern Labrador Sea, *Bulletin of the Geological Soceiety of Denmark*, *22*, 7-24.

Jones, S. M. (2003), Test of a ridge-plume interaction model using oceanic crustal structure around Iceland, *Earth and Planetary Science Letters*, *208*(3-4), 205-218.

Kristoffersen, Y., and M. Talwani (1977), Extinct triple junction south of Greenland and the Tertiary motion of Greenland relative to North America, *GSA Bulletin*, *88*(7), 1037-1049, doi:10.1130/0016-7606(1977)88<1037:ETJSOG>2.0.CO;2.

Laughton, A. (1971), South Labrador Sea and the evolution of the North Atlantic, *Nature*, *232*(5313), 612.

Louden, K. E., B. E. Tucholke, and G. N. Oakey (2004), Regional anomalies of sediment thickness, basement depth and isostatic crustal thickness in the North Atlantic Ocean, *Earth and Planetary Science Letters*, *224*(1-2), 193-211.

Macnab, R., J. Verhoef, W. Roest, and J. Arkani-Hamed (1995), New database documents the magnetic character of the Arctic and North Atlantic, *Eos, Trans. AGU*, *76*(45), 449 and 458.

Magde, L. S., and D. W. Sparks (1997), Three-dimensional mantle upwelling, melt generation, and melt migration beneath segment slow spreading ridges, *Journal of Geophysical Research: Solid Earth*, *102*(B9), 20,571-520,583.

Martinez, F., and R. Hey (2017), Propagating buoyant mantle upwelling on the Reykjanes Ridge, *Earth and Planetary Science Letters*, *457*, 10-22, doi: 10.1016/j.epsl.2016.1009.1057, doi:http://dx.doi.org/10.1016/j.epsl.2016.09.057.

Menard, H. W., and T. Atwater (1968), Changes in direction of sea floor spreading, *Nature*, *219*, 463–467.

Phipps Morgan, J., and D. W. Forsyth (1988), Three-dimensional flow and temperature perturbations due to a transform offset: Effects on oceanic crustal and upper mantle structure, *Journal of Geophysical Research: Solid Earth*, *93*(B4), 2955–2966.

Sandwell, D. T., R. D. Müller, W. H. F. Smith, E. Garcia, and R. Francis (2014), New global marine gravity model from CryoSat-2 and Jason-1 reveals buried tectonic structure, *Science*, *346*(6205), 65-67, doi:10.1126/science.1258213.

Searle, R. C., J. A. Keeton, R. B. Owens, R. S. White, R. Mecklenburgh, B. Parsons, and S. M. Lee (1998), The Reykjanes Ridge: structure and tectonics of a hot-spot-influenced, slow-spreading ridge, from multibeam bathymetry, gravity and magnetic investigations, *Earth and Planetary Science Letters*, *160*(3-4), 463-478.

Smallwood, J. R., and R. S. White (2002), Ridge-plume interaction in the North Atlantic and its influence on continental breakup and seafloor spreading, *Geological Society, London, Special Publications*, *197*(1), 15-37, doi:10.1144/gsl.sp.2002.197.01.02.

Tozer, B., D. T. Sandwell, W. H. F. Smith, C. Olson, J. R. Beale, and P. Wessel (2019), Global bathymetry and topography at 15 arc seconds: SRTM15+, *Earth and Space Science*, *in press*.

Vogt, P. R., and O. E. Avery (1974), Detailed magnetic surveys in the northeast Atlantic and Labrador Sea, *Journal of Geophysical Research: Solid Earth*, *79*(2), 363-389.

Vogt, P. R., and G. L. Johnson (1975), Transform Faults and Longitudinal Flow Below the Midoceanic Ridge, *Journal of Geophysical Research*, *80*(11), 1399-1428.

White, R. S. (1997), Rift-Plume Interaction in the North Atlantic, *Philosophical Transactions: Mathematical, Physical and Engineering Sciences*, *355*(1723), 319-339.